

EVOLUTION OF NONLINEAR α^2 -DYNAMOS AND TAYLOR'S CONSTRAINT

D. R. FEARN * and M. M. RAHMAN†

Department of Mathematics , University of Glasgow, Glasgow G12 8QW, UK

Abstract

A key nonlinear mechanism in a strong-field geodynamo is that a finite amplitude magnetic field drives a flow through the Lorentz force in the momentum equation and this flow feeds back on the field-generation process in the magnetic induction equation, equilibrating the field. We make use of a simpler nonlinear α^2 -dynamo to investigate this mechanism in a rapidly rotating fluid spherical shell. Neglecting inertia, we use a pseudo-spectral time-stepping procedure to solve the induction equation and the momentum equation with no-slip velocity boundary conditions for a finitely conducting inner core and an insulating mantle. We present calculations for Ekman numbers (E) in the range 2.5×10^{-3} to 5.0×10^{-5} , for $\alpha = \alpha_0 \cos \theta \sin \pi(r - r_i)$ (which vanishes on both inner and outer boundaries). Solutions are steady except at lower E and higher values of α_0 . Then they are periodic with a reversing field and a characteristic rapid increase then equally rapid decrease in magnetic energy. We have investigated the mechanism for this and shown the influence of Taylor's constraint. We comment on the application of our findings to numerical hydrodynamic dynamos.

Keywords: Geodynamo, α^2 -dynamo, Taylor's constraint, Earth's core.

1 Introduction

There is now a considerable literature describing hydrodynamic dynamo models (see for example the review by Fearn, 2004). However, there remains considerable merit in studying simpler models that have the benefit of isolating specific aspects of the dynamics

*Correspondence: D.Fearn@maths.gla.ac.uk, Fax: +44 (0)141 330 4111

†On leave from the Department of Mathematics, University of Dhaka, Dhaka-1000, Bangladesh

of the geodynamo process. Mean-field dynamos focus on the physics of the field generation process, parameterising the effect of small-scale and non-axisymmetric convective motions through the so-called α -effect, see Steenbeck and Krause, 1966. Such models are very suitable for studying the process of field equilibration. One aspect of this is the influence of a growing field on the convective motions responsible for generating the field. This can be modelled through a prescribed α -quenching (which decreases the strength of α as the field strength increases, see for example Roberts and Soward, 1992). We do not consider this here; α is taken to be independent of the field \mathbf{B} . We focus on a separate process in which the flow (including the so-called magnetic wind) driven by the Lorentz force feeds back on the field-generation process.

In the present paper, we make use of a nonlinear mean field dynamo model to extend earlier work and to determine the role of Taylor's constraint in a relaxation oscillation that is observed at low Ekman number and at high levels of forcing (about twice critical).

One of the fundamental results of dynamo theory is Taylor's (1963) constraint which requires that, in the limit of vanishing viscosity and inertia, the magnetic field \mathbf{B} satisfies

$$\mathcal{T}(s) \equiv \int_{C(s)} [(\nabla \times \mathbf{B}) \times \mathbf{B}]_{\phi} dS = 0, \quad \forall s. \quad (1)$$

where (s, ϕ, z) are cylindrical polar coordinates and $C(s)$ is the curved cylindrical surface of radius s , co-axial with the rotation axis, see for example the discussion in Fearn (1998). A solution satisfying (1) is known as a *Taylor state*, which is characterised by being independent of viscosity. The quantity on the left hand side of (1) can be interpreted as the net magnetic torque acting in the ϕ direction on the cylindrical shell of radius s . The above result is derived from the Navier-Stokes equation. The manner in which the system meets Taylor's constraint is subtle and this is one of the reasons that the small Ekman number limit is very difficult numerically; the fluid flow \mathbf{u} must interact with the field \mathbf{B} in the magnetic induction equation to modify \mathbf{B} in such a way that it satisfies (1). If this cannot be achieved, a significant magnetic torque acts, accelerating the azimuthal flow and inertial effects may then become important.

Close to the onset of dynamo action, the field \mathbf{B} is weak and the magnetic torque can be

balanced by viscous dissipation in Ekman boundary layers. This leads to an expression for the *geostrophic flow* of the form

$$u_G(s) \propto E^{-\frac{1}{2}} \mathcal{T}(s), \quad (2)$$

where E is the Ekman number [defined in (7)]. This balance is consistent with a weak field [$|\mathbf{B}| = O(E^{\frac{1}{4}})$, giving $\mathcal{T} = O(E^{\frac{1}{2}})$] and is known as an *Ekman state*. Malkus and Proctor (1975) first envisaged the transition from an Ekman state to a Taylor state as the strength of the mechanism driving the dynamo is increased; a significant increase in $|\mathbf{B}|$ is made possible by an increasing level of cancellation in the integral in (1) such that \mathcal{T} remains no larger than $O(E^{\frac{1}{2}})$.

Malkus and Proctor (1975) investigated theoretically the non-linear aspects of the finite amplitude behaviour of global magnetic fields and large scale flows induced by α -effect dynamos in a rotating sphere. They considered the non-linear interaction of the flow and field through the momentum equation. The boundary conditions that they considered were no-slip and an insulating mantle. The form of α was simply $\alpha = \text{const}$. They have shown that viscous and ohmic dissipative mechanisms can both play a role in determining the amplitude and structure of the flows and the evolved magnetic fields. By ignoring inertia and searching for steady solutions in the limit of small Ekman number they found two regimes; the viscous limit (the Ekman state), valid at small field amplitudes, in which viscous effects determine the final equilibration, and the inviscid limit (the Taylor state), valid for larger fields, where ohmic loss is the principal equilibrating mechanism. Determination of the geostrophic flow is an essential part of their solution in the strong field regime.

Proctor (1977) studied the above problem numerically in a rotating sphere, including inertial effects and using stress-free boundary conditions. He pointed out that the non-existence of steady solutions of Malkus and Proctor (1975) in the inviscid regime could be traced to α being independent of z , which is unrealistic. Considering $\alpha = \alpha_0 \cos \theta$, the global effects of induced velocity fields were examined. Studying only a limited set of values of the Ekman number E , Proctor (1977) has claimed that viscous and inertial forces are unimportant in the final equilibration in the limit of small E . The values of Ekman number studied were $E = 1.0, 0.01$ and 0.005 . For the latter two Ekman numbers,

the solutions were similar and thus led to the hypothesis that the system was near to an asymptotic magnetostrophic state.

Hollerbach and Ierley (1991) (hereinafter referred to as HI) studied this α^2 -dynamo again in a rotating sphere, neglecting inertial effects, and considering different forms of

$$\alpha = \alpha_0 \cos \theta f(r). \quad (3)$$

Considering first a nonlinearity only through the geostrophic flow, they focused on steady state solutions and investigated the connection between viscous and Taylor-state solutions. Their conclusions were largely the same as those of Soward and Jones (1983) who looked at a similar problem in an infinite plane-layer geometry. They then proceeded to consider the post-Taylor equilibration, incorporating the next-order ageostrophic corrections to the flow. Using a linear friction term instead of the usual Laplacian operator they presented their solution as an expansion in terms of the free decay modes of the magnetic field. For HI's choices of α some solutions do approach steady state and some do not. In all cases, Taylor-state solutions were found once α_0 exceeded the critical value α_c for the onset of dynamo action by about 10%. HI further observe that, from the evidence of the steady solutions found for mildly supercritical α , the asymptotic limit in which Taylor-state solutions are independent of E is only reached for $E \lesssim 10^{-6}$.

Barenghi (1992) took a similar α to HI and considered a spherical shell with insulating inner core. He solved the induction equation but not the full momentum equation. As did HI, he instead calculated the geostrophic flow through a modification of Taylor's constraint which balances the magnetic torque on cylinders by viscous resistance in Ekman boundary layers, see (2). This is the nonlinearity that equilibrates the dynamo in an Ekman state. If this is the only nonlinearity in the problem, then, as α_0 is increased and a Taylor state approached, the equilibrated field amplitude becomes unbounded. Other nonlinear effects are required to provide equilibration. Barenghi stops short of introducing the full momentum equation but does introduce some of the dynamics associated with the Lorentz force; the magnetic wind and stream function. He finds transition to a Taylor state when α_0 is some 13% above critical and follows his solutions to 22% above critical. In the Taylor-state regime he finds solutions independent of E .

Hollerbach and Jones (1993) (hereinafter referred to as HJ) studied an α^2 -dynamo in a

spherical shell with finitely conducting inner core and an insulating mantle. Considering $\alpha = \alpha_0 \cos \theta$ they investigated the effect of a finitely conducting inner core on dynamo solutions. They took $E = 2.5 \times 10^{-4}$ and investigated dipole solutions. They found $\alpha_c = 5.15$ and looked in detail at solutions for (a) $\alpha_0 = 5.5$ and (b) $\alpha_0 = 8$. These choices were determined by seeking to look at solutions characteristic of (a) the transition region from Ekman to Taylor states and (b) a Taylor state.

In this paper we study the model of HI in a spherical shell with a finitely conducting inner core instead of full sphere. (Barenghi, 1992, comments that this can make a qualitative difference even when the inner core is insulating.) We also use the standard viscous term throughout (instead of HI's linear friction term) and use the full Navier-Stokes equation [instead of the geostrophic flow and ageostrophic magnetic wind and stream function used by HI and Barenghi (1992)] and investigate the dependence of the equilibrated solutions on E , and the strength α_0 of α . We focus on the unsteady flow regime (not found in HJ), investigate its dependence on α_0 and E and explore the role of Taylor's constraint in the time-dependent flow found at high α_0 and low E . We explore a much greater range of supercritical α_0 than did Barenghi (1992) or HJ. Compared with HJ, we use a more realistic form (10) of α , see further discussion in Section 3.

The organization of the remainder of the paper is as follows. In Section 2, we describe our physical model with governing equations and boundary conditions. Here we also describe the solution method very briefly. Section 3 discusses the axisymmetric results of our α^2 -dynamos for our particular choice of α . Finally in Section 4 we summarise our results and present our conclusions.

2 Physical model

The model we are investigating consists of a spherical shell of inner radius r_i and outer radius r_o which is rotating about its axis with angular velocity $\boldsymbol{\Omega} = \Omega_0 \mathbf{e}_z$ (where \mathbf{e}_z denotes the unit vector in the z -direction). In all the calculations in this paper we have used $r_i = r_o/3$ consistent with the radius ratio for the Earth. The region $r_i \leq r \leq r_o$ is filled with an electrically conducting fluid of constant kinematic viscosity ν , magnetic

diffusivity η , magnetic permeability μ and density ρ_0 . Also, the exterior region $r \geq r_o$ is electrically insulating to model the Earth's mantle. The fluid outer core and the solid inner core are taken to have the same electrical conductivity, σ . The governing non-dimensional equations for the evolution of the magnetic field \mathbf{B} and fluid flow \mathbf{u} based on the scales: length, $L = r_o - r_i$; time, $\tau_\eta = L^2/\eta$; fluid velocity, $\mathcal{U} = \eta/L$; magnetic field $\mathcal{B} = (\Omega_0 \mu \rho_0 \eta)^{\frac{1}{2}}$ and pressure $\mathcal{P} = \Omega_0 L^2 / \tau_\eta$ are as follows. In the fluid outer core:

$$\frac{\partial \mathbf{B}}{\partial t} = \nabla \times (\mathbf{u} \times \mathbf{B} + \alpha \mathbf{B}) + \nabla^2 \mathbf{B}, \quad (4)$$

$$E_\eta \left[\frac{\partial \mathbf{u}}{\partial t} + (\mathbf{u} \cdot \nabla) \mathbf{u} \right] + 2\mathbf{e}_z \times \mathbf{u} = -\nabla P + (\nabla \times \mathbf{B}) \times \mathbf{B} + E \nabla^2 \mathbf{u}, \quad (5)$$

$$\nabla \cdot \mathbf{B} = 0, \quad \nabla \cdot \mathbf{u} = 0, \quad (6)$$

where P is the pressure and

$$E_\eta = \frac{\eta}{\Omega_0 L^2}, \quad E = \frac{\nu}{\Omega_0 L^2} \quad (7)$$

are the magnetic Ekman number (sometimes referred to as the Rossby number) and the Ekman number, respectively. In the finitely conducting inner core the governing equations are

$$\frac{\partial \hat{\mathbf{B}}}{\partial t} = \nabla \times (\mathbf{u}_i \times \hat{\mathbf{B}}) + \nabla^2 \hat{\mathbf{B}}, \quad (8)$$

$$\nabla \cdot \hat{\mathbf{B}} = 0, \quad (9)$$

where $\hat{\mathbf{B}}$ is the magnetic field in the inner core and $\mathbf{u}_i = \Omega_i r \sin \theta \mathbf{e}_\phi$ with Ω_i denoting the inner core angular velocity.

The α -effect in the outer core which we consider is given by

$$\alpha = \alpha_0 \cos \theta \sin \pi(r - r_i), \quad (10)$$

where α_0 is a positive real number representing the strength of α . The system loses energy through viscous and ohmic dissipation. In our model we are feeding energy into the field through the prescribed α -effect to balance these energy losses.

The flow is governed by the Navier-Stokes equation (5). The Ekman number E measures the strength of the viscous force relative to the Coriolis force. The kinematic viscosity in planetary cores is very poorly determined. A typical estimate for the Earth is $\nu = 3 \times 10^{-6} \text{ m}^2 \text{ s}^{-1}$ at the core mantle boundary (de Wijs *et al.*, 1998), giving $E = O(10^{-15})$. In this

model we do not apply the full magnetostrophic approximation (which involves setting $E_\eta = E = 0$); we retain viscous effects. Numerical considerations, however, mean that we have to accept very much larger values of E than the geophysical value.

To a good approximation, the mantle is an insulator, so the boundary condition for the field at the core mantle boundary (CMB) becomes

$$\mathbf{B} = \mathbf{B}^{(e)} \quad \text{at} \quad r = r_o, \quad (11)$$

where $\mathbf{B}^{(e)}$ is the external potential field. We are considering a finitely conducting inner core so at the inner core boundary (ICB) the field in the outer core and field in the inner core will match, so

$$\mathbf{B} = \hat{\mathbf{B}} \quad \text{at} \quad r = r_i. \quad (12)$$

For the flow we impose no slip at the boundaries. The boundary condition for the flow at the CMB becomes

$$\mathbf{u} = \mathbf{0} \quad \text{at} \quad r = r_o. \quad (13)$$

Since the inner core is rotating with an angular velocity Ω_i , the no slip velocity boundary condition at the ICB becomes

$$\mathbf{u} = \Omega_i r \sin \theta \mathbf{e}_\phi \quad \text{at} \quad r = r_i. \quad (14)$$

A freely rotating finitely conducting inner core can have a stabilizing effect on the dynamo (Hollerbach and Jones, 1993, 1995). This finitely conducting inner core couples electromagnetically with the outer core, giving rise to a magnetic torque on the inner core. The equation that determines the angular velocity of the inner core Ω_i , is the torque balance on the inner core (Glatzmaier and Roberts, 1996; Aurnou and Olson, 2000)

$$C E_\eta \frac{\partial \Omega_i}{\partial t} = E \int_S r \frac{\partial}{\partial r} \left(\frac{u_\phi}{r} \right) \Big|_{r=r_i} r_i \sin \theta dS + \int_S B_r B_\phi \Big|_{r=r_i} r_i \sin \theta dS, \quad (15)$$

where $C = \frac{8}{15} \pi r_i^5$ (considering an inner and outer core of equal density). The magnetic Ekman number E_η , which measures the ratio of the rotational timescale Ω^{-1} to the diffusive timescale τ_η , is very much larger than the Ekman number E but is still small, $O(10^{-9})$. On this basis, and consistent with many studies we will neglect inertial terms in (5). Since we are neglecting inertia in the outer core, it is consistent that we neglect it in the inner core (15) too.

The numerical code that we are using for our calculations was mainly developed by Hollerbach (see Hollerbach, 2000) and later used by Fotheringham (2000), Fotheringham *et al.* (2002). The code is well tested. Where additional code was needed we wrote and tested it ourselves. Hollerbach (2000) used a pseudo-spectral method to solve the magnetoconvection equations in a spherical geometry. He used a decomposition of \mathbf{B} and \mathbf{u} into poloidal and toroidal parts

$$\mathbf{B} = \nabla \times A \mathbf{e}_\phi + B \mathbf{e}_\phi, \quad \mathbf{u} = \nabla \times \psi \mathbf{e}_\phi + v \mathbf{e}_\phi, \quad (16)$$

(Bullard and Gellman, 1954) as they automatically satisfy the solenoidal conditions (6). He further uses KB Chebyshev polynomials in the radial direction and LB spherical harmonics in the θ direction. For most of our calculations we used truncations of 34 Chebyshev polynomials in the radial direction, 40 Legendre functions in the θ direction for both field and flow. Higher values were used to check accuracy at lower values of E . The time stepping procedure is implemented via a second order Runge-Kutta predictor-corrector method that has been modified to treat the diffusive terms implicitly. The choice of time step was continually checked to ensure the time dependence was fully resolved. For more details of the solution technique see Hollerbach (2000) and Rahman (2003).

The numerical scheme involves a time-stepping calculation of the spectral coefficients. Energies are calculated, as required, from these spectral coefficients and are a useful measure for monitoring the solutions. The magnetic energy which we calculate is

$$\begin{aligned} E_M^* &= \frac{1}{2\mu_0} \int_v |\mathbf{B}^*|^2 dv \\ &= [\rho_0 \Omega_0 \eta L^3] \frac{1}{2} \int_v |\mathbf{B}|^2 dv = [\rho_0 \Omega_0 \eta L^3] E_M, \end{aligned} \quad (17)$$

where v is the computational domain and \mathbf{B}^* is the dimensional field.

3 Results and discussion

3.1 Results and comparison with previous work

Many investigators (for example Roberts, 1972; Proctor, 1977; HJ; Fotheringham *et al.*, 2002) have used $\alpha = \alpha_0 \cos \theta$ in their investigations. This α is antisymmetric about

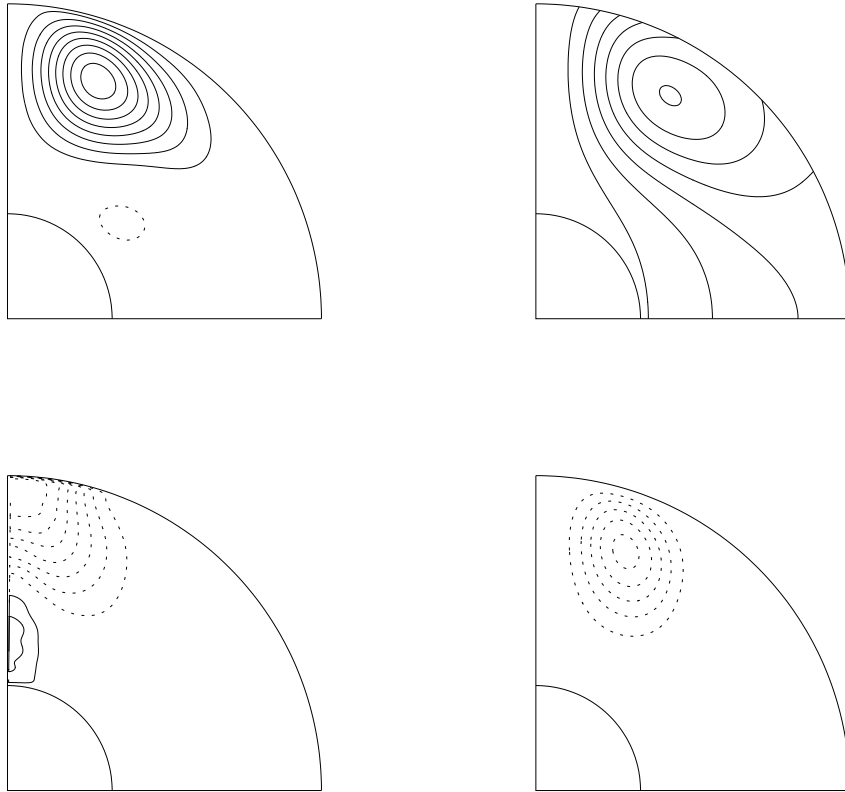


Figure 1: Contour plots of B , $Ar \sin \theta$ (top row) and $v/r \sin \theta$, $\psi r \sin \theta$ (bottom row) for the steady solution found for $\alpha_0 = 10$ and $E = 2.5 \times 10^{-4}$. Contour intervals are 0.3, 0.05, 10 and 0.1 respectively. Solid lines represent positive and dashed lines represent negative contours.

the equator and uniformly distributed radially across the outer core. Roberts (1972) studied this in his kinematic dynamo models and calculated the linear eigenfunctions. Proctor (1977) also used this choice of α in his numerical nonlinear α^2 -dynamo model. He pointed out the main advantage of this α is that magnetic fields produced by it vary slowly in space, so that only a moderate number of mesh points is necessary for an adequate representation. One disadvantage of $\alpha = \alpha_0 \cos \theta$ in our spherical shell model is that it is non zero at the inner core boundary and leads to complicated coupled boundary conditions in l and m (where l and m are the order and degree of the spherical harmonics) when the inner core is finitely conducting. One benefit of choosing our more realistic α , see (10), which has both radial and angular dependence is that we avoid this difficulty, an important improvement on HJ. Our α is antisymmetric about the equator and vanishes at both inner and outer boundaries. Chan *et al.* (2001) used the same form (10) of α in their finite element method solving for an α^2 -dynamo in a spherical shell. They did

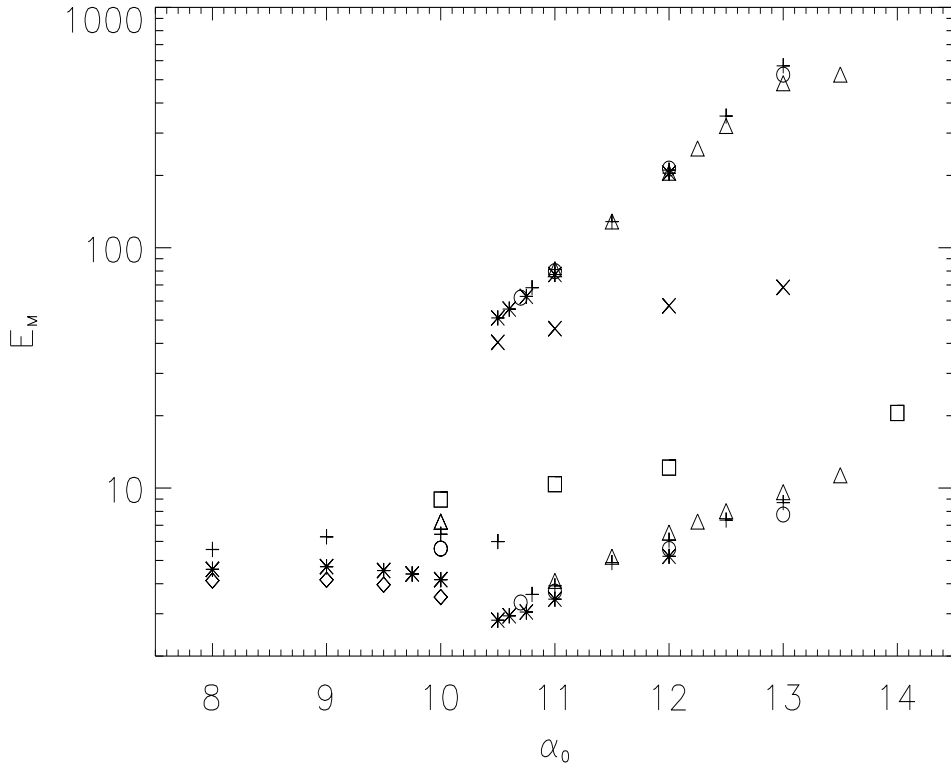


Figure 2: Magnetic energy as a function of α_0 for different values of Ekman number $E = 2.5 \times 10^{-3}(\times)$, $4.0 \times 10^{-4}(\square)$, $3.0 \times 10^{-4}(\triangle)$, $2.5 \times 10^{-4}(+)$, $2.0 \times 10^{-4}(\circ)$, $1.0 \times 10^{-4}(*)$, $5 \times 10^{-5}(\diamond)$. Single symbols represent solutions which are steady. Double symbols for a given α_0 represent the lower and upper bounds of an oscillation.

not use the momentum equation in their model, instead using α -quenching to achieve equilibration at finite field amplitude. The solutions they found were steady.

The linear onset values $\alpha_0 = \alpha_c$ for dipole and quadrupole modes corresponding to our chosen α [see (10)] are 6.69 and 6.79 respectively. The values of α_c are, of course, independent of E (since in the absence of a finite strength field, there is no force to drive a flow in (5)) and are consistent with the general features of α^2 -dynamamos noted by Steenbeck and Krause (1966) that the critical values, α_c , of dipole and quadrupole modes are always close together, see also Roberts (1972). For comparison, HJ find for their dipole mode that $\alpha_c = 5.15$ for $\alpha = \alpha_0 \cos \theta$. This lower value is consistent with there being no radial variation of α in their model.

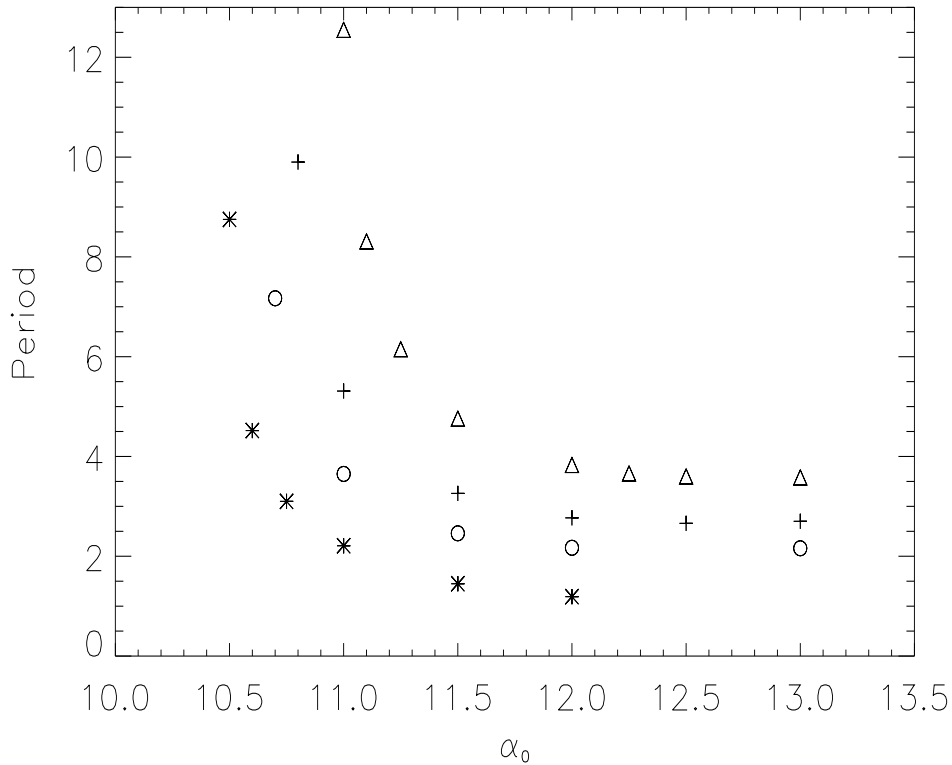


Figure 3: Period versus α_0 for different values of Ekman number $E = 1.0 \times 10^{-4}$ (*), 2.0×10^{-4} (o), 2.5×10^{-4} (+) and 3.0×10^{-4} (Δ).

The nonlinear calculations presented in this paper have used an imposed dipole parity, consider values of α_0 up to greater than $2\alpha_c$ and consider a range of values of E . We have also run a version of our code that does not impose dipole parity for a number of values of $\alpha_0 \leq 13$ and for $E = 2.5 \times 10^{-4}$. In all cases, a dipole parity solution was found. Figure 1 shows the steady solution for $\alpha_0 = 10$ and $E = 2.5 \times 10^{-4}$. It is instructive to compare Figure 1 with Figure 4 of HJ. That paper presents essentially the same calculation, except that they use $\alpha = \alpha_0 \cos \theta$. The form of the fields are very similar, though their strengths differ. The radial dependence of α appears not to be having a major influence here for these values of the parameters. HJ did not consider higher values of α_0 nor other values of E .

Figure 2 shows the dependence of our solution on E and on α_0 . For $E = 2.5 \times 10^{-3}$ we found steady behaviour for all α_0 studied ($\alpha_0 \leq 27$). Similarly for $E = 4.0 \times 10^{-4}$. At lower Ekman numbers ($E = 3.0 \times 10^{-4}$, $E = 2.5 \times 10^{-4}$, $E = 2.0 \times 10^{-4}$ and $E = 1.0 \times 10^{-4}$)

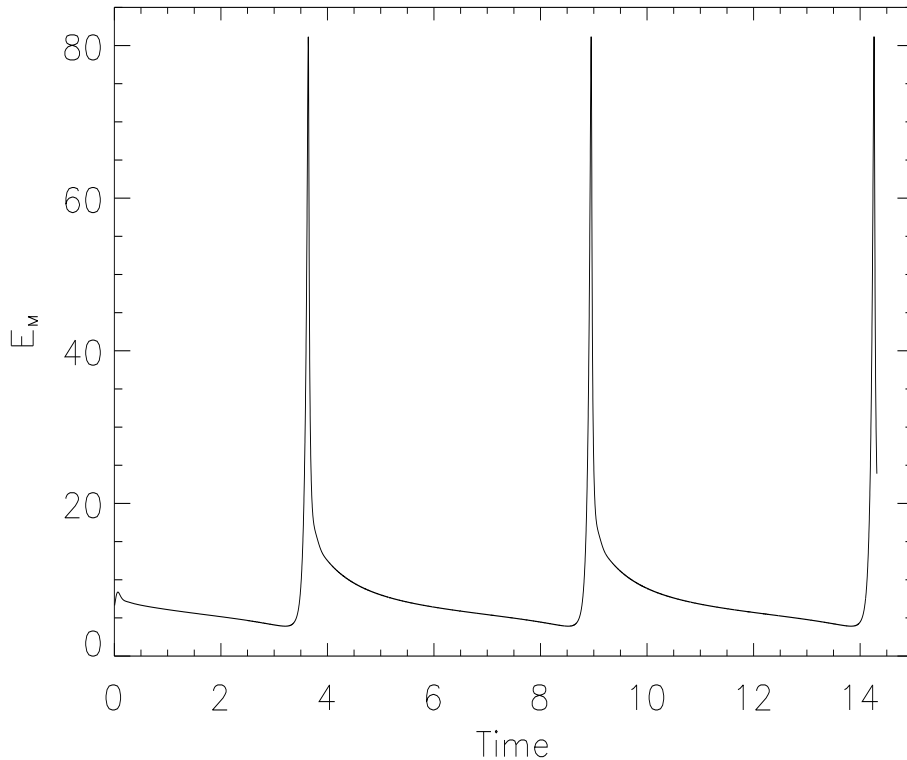


Figure 4: Magnetic energy versus time at $\alpha_0 = 11$ and $E = 2.5 \times 10^{-4}$.

steady solutions were found up to some value $\alpha_0 = \alpha_p$ of the forcing ($\alpha_p \approx 11$, $\alpha_p \approx 10.8$, $\alpha_p \approx 10.7$ and $\alpha_p \approx 10.5$ respectively). Above that value we found periodic solutions. The dependence of the period on α_0 and E is shown in Figure 3. For a given E , the period approaches a constant value as α_0 is increased and approaches infinity as α_0 is decreased. The period decreases with decreasing E . A typical periodic solution is shown in Figure 4. It can be seen that the periodic solutions are far from being simple and show a large variation in amplitude. The minimum and maximum values are indicated in Figure 2. The sharpness of the peaks observed in Figure 4 varies with α_0 and E . For a fixed E the peaks become sharper as α_0 increases. The sharpness of the peaks decreases as E increases when α_0 is fixed. Larger values of α_0 and smaller values of E are therefore more difficult to explore numerically.

A similar behaviour was found by HI who found that, for some choices of the radial dependence of α , steady solutions gave way to oscillatory solutions as α_0 was increased. The r -dependences of α which they considered were the two one parameter families, $f(r) = f_1(r) = \tanh(rq_1)/\tanh q_1$ and $f(r) = f_2(r) = \tan(r \tan^{-1} q_2)/q_2$. For example,

for $q_1 = \infty$ and $q_2 = 2$ they observed this sharp peak oscillatory behaviour which they attributed to instability of the toroidal field. We discuss the oscillatory behaviour in detail in Section 3.2.

HI's solutions were found using their linear friction whose strength is measured by their parameter E' and neither their period nor amplitude were found to depend significantly on E' in the asymptotic limit of small E' . Our results show the amplitude to be fairly insensitive to E (see Figure 2 and further discussion in Section 3.2) though the period shows a significant dependence on E (see Figure 3) *for the range of E explored*. With solutions steady for $E = 4 \times 10^{-4}$, plotting the values shown in Figure 3 for, say, $\alpha_0 = 12$ versus E shows they are entirely consistent with the period approaching a constant value in the limit of $E \rightarrow 0$. HI comment that the asymptotic limit is found in their case only when $E \lesssim 10^{-6}$.

Looking again at Figure 2 we observe that, for all solutions, the magnetic energy increases with increasing α_0 except for values of α_0 just below the onset at $\alpha_0 = \alpha_p$ of oscillatory behaviour. In this region, the magnetic energy decreases with increasing α_0 . In general, the variation of magnetic energy with E is modest and consistent with HI's comments that the truly inviscid regime is only reached for values of $E \lesssim 10^{-6}$. The variation in α_p with E and the decrease in E_M with α_0 in the vicinity of $\alpha_0 \lesssim \alpha_p$ exacerbates the apparent variation of E_M with E around $\alpha_0 = 10$.

The behaviour observed here differs from that found by HI in a number of respects but there are also important similarities. In their Figure 8 and Figure 9, for steady fields ($\alpha_c < \alpha_0 < \alpha_p$), they show the behaviour of the equilibrated energy E_M versus α_0 for a range of values of E' and for two different choices of $f(r)$. In their Figure 8, the solution is viscously controlled (with E_M increasing with E') except where α_0 is close to α_p where E_M is independent of E' but increases significantly with α_0 . In their Figure 9, the viscously controlled solution is unstable and it is the large amplitude (close to Taylor state) solution which is stable. This shows an increase in E_M with decreasing E' , approaching a constant value and a significant increase of E_M with α_0 except very close to α_p where there is very slight decrease. The convergence to to an E' -independent behaviour is noticeably much worse close to α_p . The latter features more closely mirror

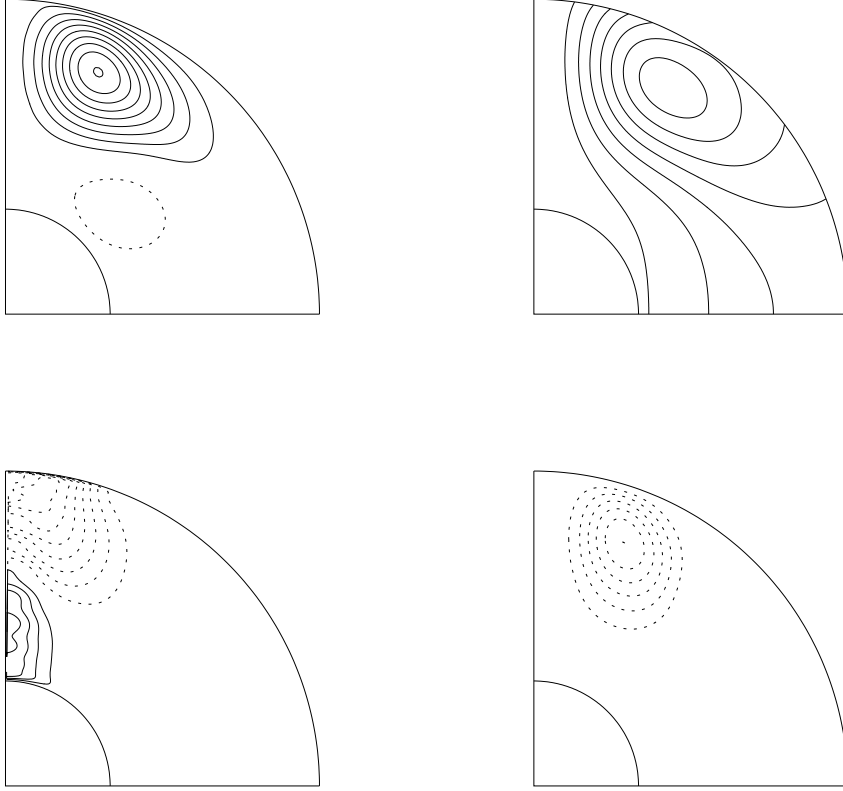


Figure 5: Snapshot of the solution for $\alpha_0 = 11$ in the slow decay phase for $E = 2.5 \times 10^{-4}$ at $E_M = 8$. Contour intervals are 0.3, 0.05, 10 and 0.1 respectively. Solid lines represent positive and dashed lines represent negative contours.

what we observe but the variation in E_M with E' is opposite to that we see in Figure 2.

3.2 Oscillation mechanism

We wish to understand more about the mechanisms that lead to the observed periodic behaviour for $\alpha_0 > \alpha_p$; a rapid increase in E_M followed by a rapid decrease then a much slower decay.

In the slow decay phase, there is only modest change in the form of the solution. An example is shown in Figure 5. This closely resembles that shown in Figure 1 for the steady solution found for $\alpha_0 < \alpha_p$. This suggests that, in this part of the cycle, what we are seeing is essentially the steady solution, but slowly decaying (there being no steady solution for $\alpha > \alpha_p$).

We now proceed to consider the rapid growth phase. Figure 6 shows 5 snapshots covering



Figure 6: Contour plots of the field B (1st column), $Ar \sin \theta$ (2nd column), the flow $v/r \sin \theta$ (3rd column) and $\psi r \sin \theta$ (4th column) at five times: $t_0, t_0 + 0.4, t_0 + 0.8, t_0 + 0.9, t_0 + 1.0$ (top to bottom) for $\alpha_0 = 11$ and $E = 2.5 \times 10^{-4}$. The corresponding magnetic energies are $E_M = 4.80, 4.26, 4.68, 8.80$ and 41.0 . The minimum of $E_M \approx 3.99$ is at about $t_0 + 0.62$. Contour intervals are 0.5, 0.05, 10 and 0.1 respectively. Solid lines represent positive and dashed lines represent negative contours.

the end of the slow decay phase and its evolution into the rapid growth phase. A key feature to observe is the reversal of the field and the evolution of the flow to be almost geostrophic (i.e. independent of z). The strong growth of the field is then accompanied by a decay in the geostrophic flow, leaving only a weak magnetic wind.

We compared the growth rate in the rapidly growing phase with the corresponding linear growth rate. Specifically, we took the end point of an integration, with $E_M = 8.8$. This solution is shown in the fourth row of Figure 6. Integrating onwards, the growth rate was found to be 10.9. We then took the same solution for the field and reduced its amplitude by a factor 10^{10} . This was then used as the initial condition for a short integration to determine the linear growth rate (the reduction in field amplitude results in a reduction in the flow amplitude by 10^{20} , so there is negligible flow). The linear growth rate was found to be 11.1, very close indeed to the nonlinear growth rate. This is convincing evidence that the reason for the rapid growth observed is that there is little equilibration of field amplification by the flow. We expect the linear growth rate to increase with α_0 . This is consistent with the observed increase in sharpness of the peaks with increasing α_0 . It is probably relevant that the azimuthal flow is predominantly geostrophic. It is the geostrophic flow that has the role of modifying the field in such a way that Taylor's constraint is satisfied while the magnetic wind, which is clearly weak here, is responsible for equilibrating the field strength in a Taylor state. We say more about the role of Taylor's constraint in Section 3.3.

The transition from the rapid growth phase to the rapid decay phase is illustrated in Figure 7. This sequence follows on immediately from those in Figure 6, but are much more closely spaced in time to capture the rapid changes. Note that the contour intervals chosen for this figure are larger than those for Figure 6. Following the maximum magnetic energy (row 2) there is a rapid fall-off in the strength of the azimuthal field and a much slower weakening of the meridional field. The meridional flow follows the azimuthal field quite closely. The most dramatic changes are in the differential rotation (column 3). We discuss this evolution further in Section 3.3.

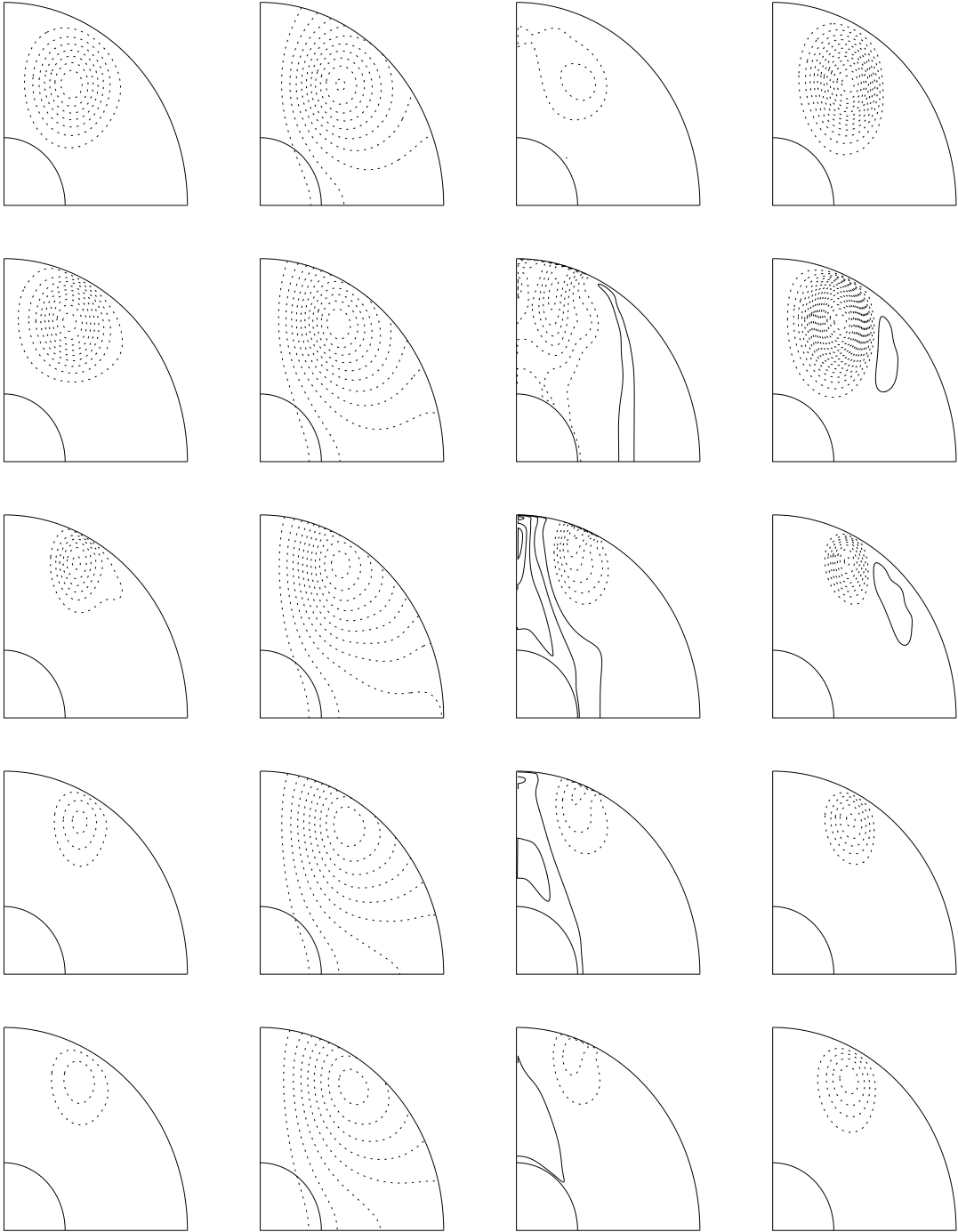


Figure 7: Contour plots of the field B (1st column), $Ar \sin \theta$ (2nd column), the flow $v/r \sin \theta$ (3rd column) and $\psi r \sin \theta$ (4th column) at five times: $t_0 + 1.02, t_0 + 1.04$ (maximum of E_M), $t_0 + 1.06, t_0 + 1.08, t_0 + 1.1$ (top to bottom) for $\alpha_0 = 11$ and $E = 2.5 \times 10^{-4}$. The corresponding magnetic energies are $E_M = 59.9, 80.5, 48.2, 29.2$ and 22.0 . Contour intervals are 1.0, 0.1, 20 and 0.2 respectively. Solid lines represent positive and dashed lines represent negative contours.

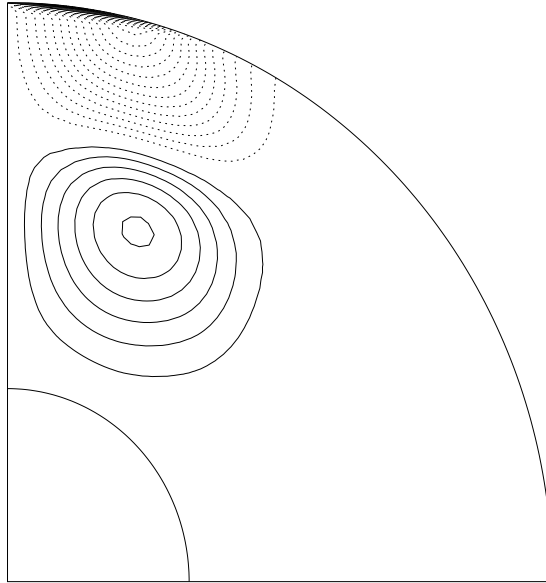


Figure 8: Contour plots of $[(\nabla \times \mathbf{B}) \times \mathbf{B}]_\phi$ at $\alpha_0 = 10$ for Ekman numbers, 2.5×10^{-4} . Contour interval is 1. Solid lines represent positive and dashed lines represent negative contours.

3.3 Taylor's constraint

We now investigate in detail the influence of Taylor's constraint. In a model in which viscous terms are retained (with E small) it is often instructive to have a simple measure of the extent to which a solution satisfies (1). A key point is the extent to which regions of positive $[(\nabla \times \mathbf{B}) \times \mathbf{B}]_\phi$ cancel with regions of negative $[(\nabla \times \mathbf{B}) \times \mathbf{B}]_\phi$ in the integral. The quantity

$$T(s) = \frac{\int_{C(s)} [(\nabla \times \mathbf{B}) \times \mathbf{B}]_\phi dS}{\max \int_{C(s)} |[(\nabla \times \mathbf{B}) \times \mathbf{B}]_\phi| dS}. \quad (18)$$

is a measure of this. Figure 8 shows the contour plots of $[(\nabla \times \mathbf{B}) \times \mathbf{B}]_\phi$ in the steady state for Ekman number $E = 2.5 \times 10^{-4}$ and $\alpha_0 = 10$. From this figure it is clear that a lot of cancellation is going on between the positive and negative regions. Corresponding plots for $E = 4.0 \times 10^{-4}$, 3.0×10^{-4} , 2.0×10^{-4} and 1.0×10^{-4} at $\alpha_0 = 10$ are all similar (see Rahman, 2003).

In Figure 9, we have plotted $T(s)$ for each of the solutions illustrated in Figure 6. We

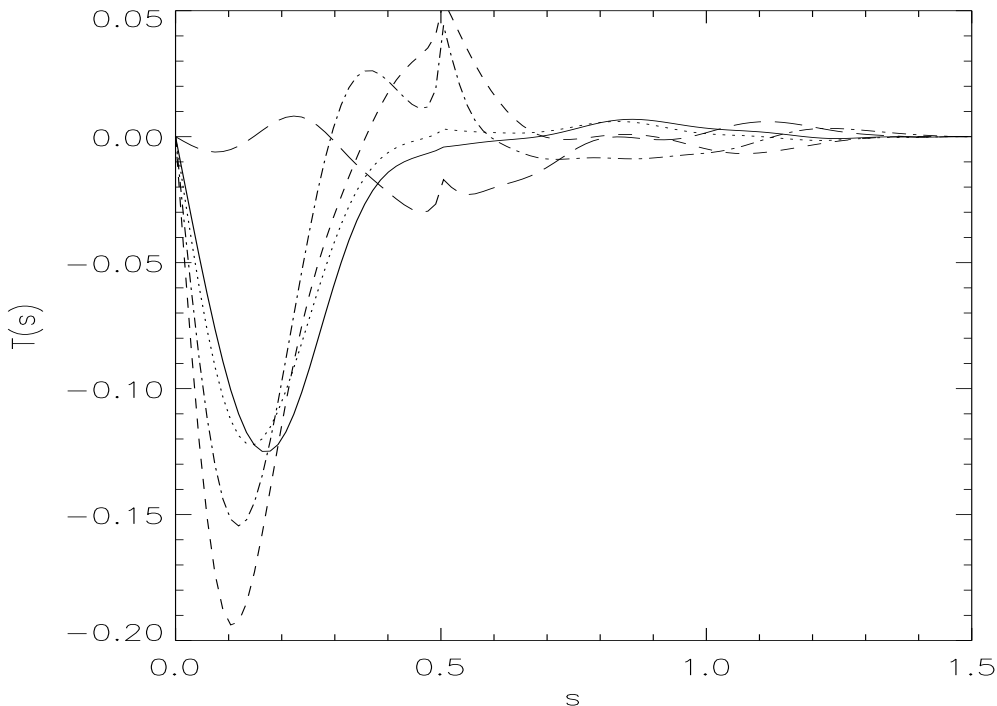


Figure 9: T versus s at $\alpha_0 = 11$ and $E = 2.5 \times 10^{-4}$ corresponding to the solutions plotted in Figure 6: t_0 (full line), $t_0 + 0.4$ (dotted line), $t_0 + 0.8$ (dashed line), $t_0 + 0.9$ (dash-dot line) and $t_0 + 1.0$ (long-dash line).

observe that initially ($t_0 \rightarrow t_0 + 0.4$) there is little change as we approach the minimum energy. Thereafter there is a significant increase in $T(s)$, followed by a rapid decrease between $t_0 + 0.8$ and $t_0 + 1.0$. The decrease in $T(s)$ is accompanied by a decrease in the geostrophic flow and increase in field strength, see Figure 6.

In Section 3.2, we compared the growth rate in the rapidly growing phase with the linear growth rate and found them comparable. In a further test we looked at the extent to which Taylor's constraint is satisfied. The situation is shown in Figure 10; Taylor's constraint is well satisfied by the initial condition and by the nonlinear solution at the later time. By contrast, it is clearly not satisfied by the linear solution at the later time. Hence, while the flow is not having a major influence in constraining the growth of the field, it clearly is influencing the field sufficiently to ensure that Taylor's constraint continues to be satisfied.

The variation in $T(s)$ corresponding to Figure 7, the transition from the rapid growth to

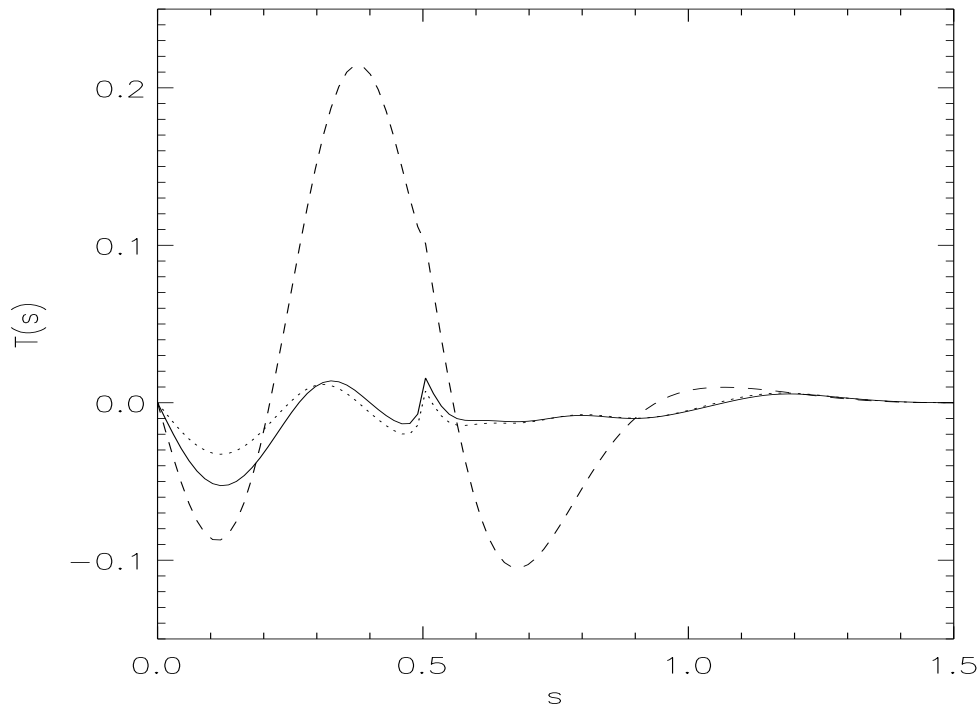


Figure 10: T versus s at $\alpha_0 = 11$ and 2.5×10^{-4} at time $t_0 + 0.93$ ($E_M = 12.78$)(full line) and $t_0 + 0.94$ for the nonlinear case ($E_M = 14.75$)(dotted line) and the linear case ($E_M = 14.90 \times 10^{-20}$)(dashed line).

the rapid decay phases, is illustrated in Figure 11. Taylor's constraint is well satisfied on the upward slope of the peak, consistent with the rapid growth in field energy. As the peak is approached, the system is clearly unable to continue to satisfy (1) nearly so well. There is a dramatic increase in $T(s)$ accompanied (see Figure 7) by a rapid increase in the differential rotation and decrease in the azimuthal field strength. HI observe that the azimuthal field B seems to collapse first and the meridional field A only drops off later. This is exactly what we see here and exactly what one would expect if the collapse is caused by a breakdown of Taylor's constraint inducing a large geostrophic flow since it acts back only on B .

There is clear evidence from Figure 11 that, as the field strength weakens, the system is recovering, with $T(s)$ reducing again towards the values observed in the slow decay phase. The field continues to decay but much less dramatically, eventually reversing and then repeating the whole cycle.

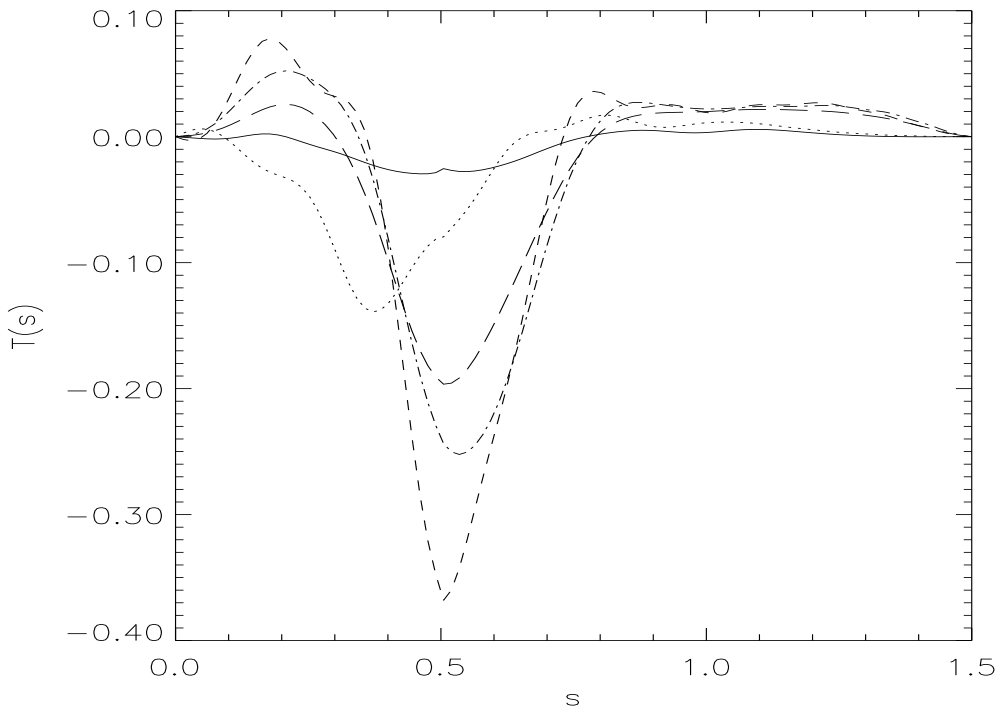


Figure 11: T versus s at $\alpha_0 = 11$ and $E = 2.5 \times 10^{-4}$ corresponding to the solutions plotted in Figure 7: $t_0 + 1.02$ (full line), $t_0 + 1.04$ (dotted line), $t_0 + 1.06$ (dashed line), $t_0 + 1.08$ (dash-dot line) and $t_0 + 1.1$ (long-dash line).

3.4 The role of E

In Section 3.1 we made a few comments about how our solutions varied with E and found them to be consistent with becoming independent of E in the limit $E \rightarrow 0$ as we would expect of a Taylor state. Here we look at the behaviour with E in more detail.

Figure 12 shows a plot of T versus s for different Ekman numbers in the steady state at $\alpha_0 = 10$. We see there is a clear trend that as E reduces, T is tending to zero. From Figure 13 we see that the way it is approaching zero is $T = O(E^{0.495})$. The exponent 0.495 has been calculated based on the least-square fit of the data. The above shows there is strong indication that T is tending to zero as $E^{\frac{1}{2}}$. This is consistent with the system being in a Taylor state (with only small viscous modifications), see Malkus and Proctor (1975), equation (5.12), see also Rüdiger and Hollerbach(2004).

For comparison with Figure 6 ($E = 2.5 \times 10^{-4}$) we have plotted the corresponding solution snapshots for $E = 10^{-4}$ in Figure 14. The accompanying plots for $T(s)$ are in Figure 15.

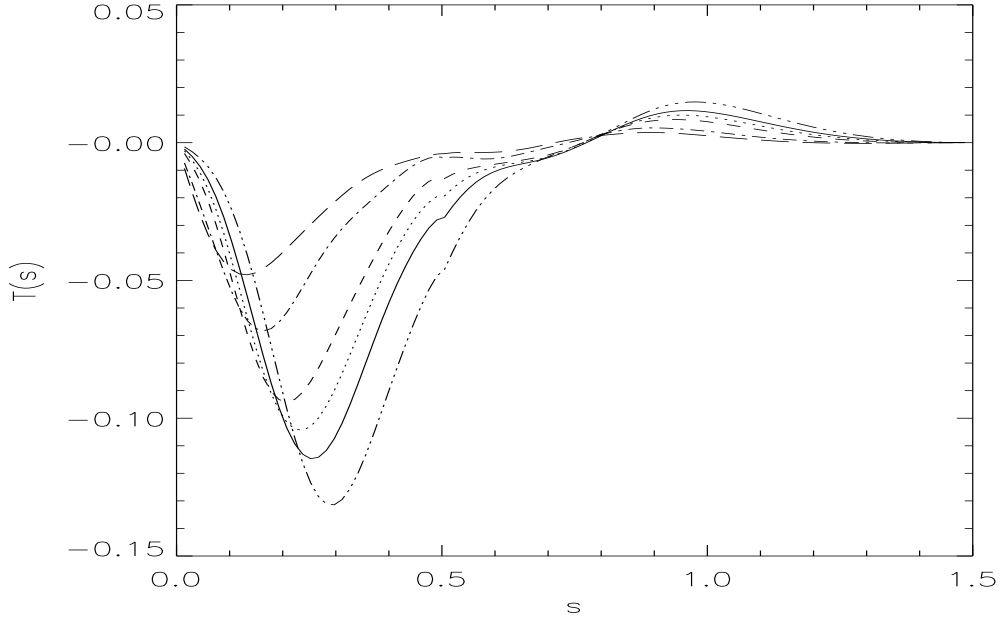


Figure 12: T versus s at $\alpha_0 = 10$ for different values of Ekman number $E = 4.0 \times 10^{-4}$ (dash dot dotted line), 3.0×10^{-4} (solid line), 2.5×10^{-4} (dotted line), 2.0×10^{-4} (dashed line), 1.0×10^{-4} (dash dotted line) and 5.0×10^{-5} (long dashed line).

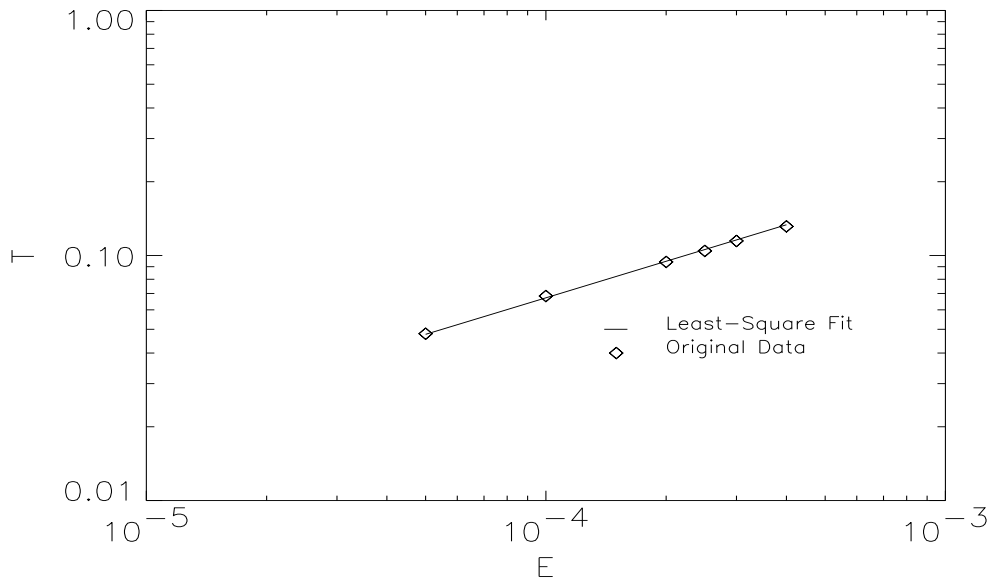


Figure 13: The maximum modulus T of $T(s)$ in Figure 12 versus E at $\alpha_0 = 10$. The behaviour is very close to $T \propto E^{\frac{1}{2}}$, see text.



Figure 14: For comparison with Figure 6; contour plots of the field B (1st column), $Ar \sin \theta$ (2nd column), the flow $v/r \sin \theta$ (3rd column) and $\psi r \sin \theta$ (4th column) at five times $t_0, t_0 + 0.4, t_0 + 0.8, t_0 + 0.9, t_0 + 1.0$ (top to bottom) before for $\alpha_0 = 11$ and $E = 10^{-4}$. The corresponding magnetic energies are $E_M = 4.46, 3.57, 4.07, 9.20$ and 55.7 . The minimum of $E_M \approx 3.33$ is at about $t_0 + 0.61$. Contour intervals are 0.5, 0.05, 10 and 0.1 respectively. Solid lines represent positive and dashed lines represent negative contours.

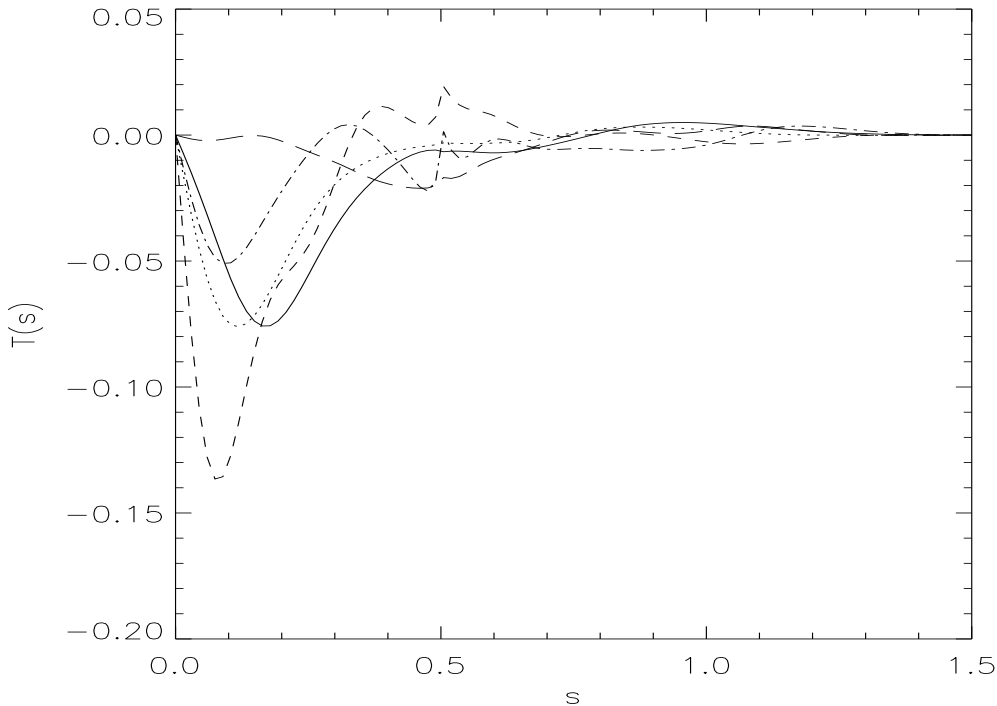


Figure 15: For comparison with Figure 9; T versus s at $\alpha_0 = 11$ and $E = 10^{-4}$ corresponding to the solutions plotted in Figure 14: t_0 (full line), $t_0 + 0.4$ (dotted line), $t_0 + 0.8$ (dashed line), $t_0 + 0.9$ (dash-dot line) and $t_0 + 1.0$ (long-dash line).

We observe that reducing the Ekman number by a factor of 2.5 has led little change in the solution in the phase where there is the transition from slow decay to rapid growth; Figures 6 and 14 are very similar. Similarly, we observe exactly the same features in Figures 9 and 15, especially when one takes into consideration that the snapshots do not necessarily capture identical points in the evolution of the two cases. The key feature is a $T(s)$ in the slow decay phase that is comparable with that for the steady mode at $\alpha_0 = 10$ (see Figure 12). This begins to increase about the minimum of E_M , then subsequently decreases dramatically to a value well below that of the slow decay phase. Consistent with the lower value of E , $T(s)$ is systematically much smaller in magnitude in Figure 15 compared with Figure 9

In the above discussion we have identified the role of Taylor's constraint in the relaxation oscillation observed for small E and large α_0 . The key qualitative features of the oscillation are the same as those found by HI for a full sphere, linear friction and different choices of the radial dependence of α . As with their results, the ratio of the maximum to minimum magnetic energy is in the range 10-20 (though this increases a little with α_0). For the range of values of E we have studied, the maximum of E_M is virtually

independent of E while there is only a very weak dependence of the minimum of E_M with E . This is in stark contrast to the steady mode observed for higher E where E_M increases significantly with E , see Figure 2. As with our earlier discussion at the end of Section 3.1, the very modest variation of the minimum of E_M with E is consistent with E_M becoming independent of E in the limit of $E \rightarrow 0$.

4 Conclusions

In our study of nonlinear α^2 -dynamo in a spherical shell we have investigated the evolution of the mean field and its dependence on α_0 and E using an α -effect that vanishes on both inner and outer boundaries. We found solutions for Ekman numbers in the range $E = 2.5 \times 10^{-3} - 5.0 \times 10^{-5}$. For $E \geq 4 \times 10^{-4}$ all solutions remain steady. The magnetic energy E_M increases as α_0 increases or as E increases. For $E \leq 3 \times 10^{-4}$ solutions are steady for $6.69 < \alpha_0 < \alpha_p(E)$ and an unsteady reversing solution is found for $\alpha_0 \geq \alpha_p$. The solution has a sudden rise and subsequent rapid fall in the magnetic energy, followed by a period of slow decay. The latter phase resembles closely the steady phase found at lower α_0 or higher E . The magnetic energy E_M increases as α_0 increases, but there is only a modest influence of E on E_M .

We have investigated the nature of the periodic solutions and particularly the role of Taylor's constraint. All evidence is that we are dealing with a solution that is in a Taylor state; the differential rotation is not dominated by the geostrophic flow (as would be the case in an Ekman state) and solutions are consistent with becoming independent of E at leading order in the limit of small E . At a given value of E , the extent to which Taylor's constraint is satisfied varies during the cycle. At the start of the rapid growth phase, there is an increase in $T(s)$ close to the axis and the flow is predominantly geostrophic briefly. As field growth continues (at a rate very close to the linear growth rate), $T(s)$ then decreases significantly in magnitude to its lowest amplitude. The magnetic wind is weak at this point so exerts little constraint on the growth of the field, but the geostrophic flow exerts sufficient influence to maintain (indeed improve) the extent to which Taylor's constraint is satisfied. This situation continues to close to the peak of magnetic energy where the system is no longer able to maintain this balance, and $T(s)$ increases dramatically to its

maximum value accompanied by an increase in the azimuthal flow and accompanying decrease in the azimuthal field.

The unusual periodic behaviour found and analysed here has not been found in similar calculations (for example Hollerbach and Jones, 1993) for simpler forms of α (independent of r). They chose $\alpha = \alpha_0 \cos \theta$. Rahman(2003) extended their results up to $\alpha_0 = 27$ and found all solutions steady. Rahman (2003) did find unsteady solutions for choices of $f(r)$ other than that used here. Unsteady solutions have also been found for radially dependent α by HI in a full sphere using linear friction, indicating that the mechanism is not particular to the choice of radial dependence that we have chosen, the form of friction nor the presence of the inner core. We argue that the more general form of α used here is more realistic.

The rapid time dependence of the periodic solutions suggests that the neglect of inertia may not be valid, at least during part of the cycle. Fearn and Rahman (2004) have investigated this and found that, for $E = 2.5 \times 10^{-4}$, the addition of inertial effects restore a steady solution when $E_\eta \gtrsim 10^{-2}$. This corresponds to a magnetic Prandtl number $P_m (= E/E_\eta = \nu/\eta) \lesssim 2.5 \times 10^{-2}$. How these values of E_η or P_m depend on E has not been investigated. It is therefore difficult to predict how this work relates to the Earth ($E_\eta \approx 10^{-9}$, $P_m \approx 10^{-6}$). What is clearer is its relevance to numerical geodynamo models. These typically have E comparable with the value used here and rarely have P_m less than 0.1. Consequently, though the dynamics, incorporating convectively driven flows, is certainly more complex, we might expect that the relaxation type oscillation observed here may be present in numerical dynamo models.

Acknowledgements

We would like to thank Dr. Paul Fotheringham for providing his code and Dr. Rainer Hollerbach for many helpful discussions of the problem. Additionally, discussions with Prof. Andrew Soward and the comments of two anonymous referees have helped considerably in improving the presentation of our results. Mohammad M. Rahman is grateful to Glasgow University and ORS for funding through a research studentship.

References

- Aurnou, J. and Olson, P., "Control of inner core rotation by electromagnetic, gravitational and mechanical torques," *Phys. Earth Planet. Inter.* **117**, 111-121 (2000).
- Barenghi, C.F., "Nonlinear planetary dynamos in a rotating spherical shell. II. The post-Taylor equilibration for α^2 -dynamos," *Geophys. Astrophys. Fluid Dynam.* **67**, 27-36 (1992).
- Bullard, E. C. and Gellman, H., "Homogeneous dynamos and terrestrial magnetism," *Phil. Trans. R. Soc. Lond. Ser. A* **247**, 213-278 (1954).
- Chan, K. H., Zhang, K., Zou, J. and Schubert, G., "A non-linear, 3-D spherical α^2 dynamo using a finite element method," *Phys. Earth Planet. Inter.* **128**, 35-50 (2001).
- de Wijs, G. A., Kresse, G., Vocadlo, L., Dobson, D., Alfe, D., Gillan, M. J. and Price, G. D., "The viscosity of liquid iron at the physical conditions of the Earth's core," *Nature*. **392**, 805-807 (1998).
- Fearn, D. R., "Hydromagnetic flow in planetary cores," *Rep. Prog. Phys.* **61**, 175-235 (1998).
- Fearn, D. R., "The geodynamo," in *Mathematical aspects of natural dynamos* (E. Dormy, ed.) (2004).
- Fearn, D.R. and Rahman, M.M., "The role of inertia in models of the geodynamo," *Geophys. J. Int.* submitted (2004).
- Fotheringham, P., "A numerical study of magnetic and non-magnetic geophysical fluid dynamics" *Ph.D. Thesis*. University of Glasgow (2000).
- Fotheringham, P., Fearn, D. R. and Hollerbach, R., "Magnetic stability and nonlinear evolution of a selection of mean field dynamos" *Phys. Earth Planet. Inter.* **134**, 213-237 (2002).
- Glazmaier, G. A., and Roberts, P. H., "Rotation and magnetism of Earth's inner core," *Science* **274**, 1887-1891 (1996).
- Hollerbach, R., "A Spectral solution of the magnetoconvection equations in a spherical geometry," *Int. J. Num. Mech. Fluids.* **32**, 773-797 (2000).
- Hollerbach, R. and Ierley, G., "A modal α^2 -dynamo in the limit of asymptotically small viscosity," *Geophys. Astrophys. Fluid Dynam.* **56**, 133-158 (1991). [Referred to as HI in text.]
- Hollerbach, R. and Jones, C. A., "A geodynamo model incorporating a finitely conducting inner core," *Phys. Earth Planet. Inter.* **75**, 317-327 (1993). [Referred to as HJ in text.]
- Hollerbach, R. and Jones, C. A., "On the magnetically stabilizing role of the earth's inner core," *Phys. Earth Planet. Inter.* **87**, 171-181 (1995).
- Malkus, W. V. R. and Proctor, M. R. E., "The macrodynamics of α -effect dynamos in rotating

- fluids,” *J. Fluid Mech.* **67**, 417-443 (1975).
- Proctor, M. R. E., “Numerical solutions of the nonlinear α -effect dynamo equations,” *J. Fluid Mech.* **80**, 769-784 (1977).
- Rahman, M. M., “Evolution and stability of nonlinear mean field dynamos,” *Ph.D. Thesis*, University of Glasgow (2003).
- Roberts, P. H., “Kinematic dynamo models,” *Phil. Trans. R. Soc. Lond. Ser. A* **272**, 633-703 (1972).
- Roberts, P. H. and Soward, A. M., “Dynamo theory,” *Ann. Rev. Fluid Mech.* **24**, 459-512 (1992).
- Rüdiger, G and Hollerbach, R., *The magnetic universe: geophysical and astrophysical dynamo theory*, Wiley VCH, Berlin (2004).
- Soward, A.M. and Jones, C.A., “ α^2 -dynamos and Taylor’s constraint,” *Geophys. Astrophys. Fluid Dynam.* **27**, 87-122 (1983).
- Steenbeck, M., Krause, F., “The generation of stellar and planetary magnetic fields by turbulent dynamo action,” *Z. Naturforsch.* **21a**, 1285-1296 (1996).
- Taylor, J. B., “The magnetohydrodynamics of a rotating fluid and the Earth’s dynamo problem,” *Proc. R. Soc. Lond. Ser. A* **274**, 274-283 (1963).